Dynamics of self-trapped beams with phase dislocation in saturable Kerr and quadratic nonlinear media

Dmitry V. Skryabin* and William J. Firth
Department of Physics and Applied Physics, John Anderson Building, University of Strathclyde, 107 Rottenrow, Glasgow, G4 0NG, Scotland
(Received 11 May 1998)

We present a detailed stability analysis of one- and two-ring solitary waves with central phase dislocation in self-focusing saturable and quadratic nonlinear media. Varying parameters, we demonstrate transitions between different filamentation scenarios. An analytical approach is developed for the study of filament dynamics after ring breakup. Approximate expressions for the angular separation rate of filaments based on the conservation of the angular momentum and on the conservation of the Hamiltonian are derived and compared. The stability analysis and analytical results are tested by an extensive series of numerical simulations of the original models, and good agreement is found. [S1063-651X(98)14609-3]

PACS number(s): 42.65.Tg, 42.65.−k

I. INTRODUCTION

Solitary wave effects due to optical propagation in nonlinear media have been a very active area of theoretical and experimental research ever since self-trapping of an optical beam due to nonlinear change of refractive index was predicted in the 1960s [1]. For review of the early works see, e.g., [2,3]. The basic model that was studied is the nonlinear Schrödinger equation (NLS), which can be derived from the Maxwell equations for centrosymmetric nonlinear media in the quasioptical limit. The NLS is of great importance not only in nonlinear optics but in most branches of nonlinear science [2,3].

Both bright and dark spatial solitary solutions of the one-dimensional (1D) NLS are also exact solutions of the NLS in two transverse dimensions (2D), but both are subject to a transverse modulational instability (MI) which develops along the second transverse coordinate [3,4]. This instability results in breakup of a bright solitary stripe into a set of filaments in the self-focusing case [3], while a vortex chain forms from a dark solitary stripe in self-defocusing media [4]. These vortices are dark holes, with a nested phase dislocation of order l at their core, on a bright, stable, background which is infinite (in theory) or sufficiently wide (in practice), where l is any positive or negative integer. All vortices of order two or more (i.e., $|l|\geqslant 2$) are unstable, breaking up into vortices with $|l|=1$, which are stable for topological reasons. Optical vortices are themselves a subject of great interest: for an excellent recent review of dark solitons and vortices see [5].

During recent years propagation and MI of bright and dark solitary waves have been extensively studied not only in the NLS context, i.e., in Kerr-like media, but also in the quadratically nonlinear and photorefractive media; see, e.g., [6–11]. Linear propagation of the beams with phase dislocations and the related angular momentum effects have also been a very active area of research [12,13].

The present paper deals with 2D propagation of electromagnetic waves in self-focusing saturable and in quadratic nonlinear media. Bright solitary waves decaying monotonically with distance from the axis (ground states) are the most important solitary solutions in these media, but they do not exhaust the set of self-trapped solutions. Considering 2D NLS with pure cubic nonlinearity Gagnon and Paré [14] built two remarkable sets of analytic solutions. These sets are analogs of Hermite-Gaussian and Laguerre-Gaussian modes of the propagation equation in linear media [15]. In a certain limit these ''nonlinear modes,'' which generally depend on the longitudinal coordinate, transform into self-trapped solutions [14]. Several types of solitary waves reported by different authors, e.g., with a bright central spot and one or more radial nodes [16], ''doughnut'' solutions with a nested phase dislocation [17], the ''dipole'' solution [18], and solutions with both radial and azimuthal nodes [19], are apparently special cases of these ''nonlinear modes'' built by Gagnon and Paré. It is natural to expect that analogs of these solutions can exist in models that in certain limits are close to the NLS. Indeed, solutions with a *bright* central spot and radial nodes have been studied in saturable [20,21] and quadratic nonlinear media [22–24]. Solutions with a *dark* central spot and nested phase dislocation have been also reported in both saturable [25–29] and quadratic [22,23,28] media.

The stability of these solutions is a nontrivial issue because the standard stability criterion for the ground states [20] is only a necessary condition for the stability of higher-order solutions with nodes, and has no relevance to MI. It was first shown for saturable nonlinearity [21] that many-ring solutions with a bright central spot are stable with respect to purely radial perturbations but unstable with respect to azimuthally dependent perturbations, showing breakup of their rings into filaments. Similar solutions in quadratic nonlinear media show not only symmetry-breaking azimuthal instability, in analogy with saturable media, but also a novel symmetry-preserving decay scenario, which is absent for the ground-state quadratic solitons [24].

Note that, while the MIs of the ring and stripe solitary waves have much in common, there is an important difference between them. Stripes typically have a continuum of

*Electronic address: dmitry@phys.strath.ac.uk

unstable eigenmodes spanning a finite range of wave numbers. In contrast rings have a discrete set of unstable eigenmodes because of the phase periodicity condition.

Our special interest here is in self-trapped solutions with phase dislocation surrounded by one or more bright rings. Breakup of these rings into filaments has been reported in [23,25–29]. Existence of these solutions in quadratic nonlinear media and rigorous stability analysis for both saturable and quadratic media were reported by us in [28]. In this work we study the filament dynamics after the breakup (dynamics here and below means evolution in z as the beam propagates). This dynamics is strongly affected by the fact that, due to the phase dislocation, these beams have nonzero orbital angular momentum. Like free Newtonian particles, filaments fly off tangential to the initial ring, vividly demonstrating conservation of orbital angular momentum in their motion [28].

Experimental observations of filamentation of the finite beams with a nested phase dislocation has been recently reported for the self-focusing saturable [30,31] and photorefractive [11] media. The spatial profiles of the input beams used in these experiments did not correspond to self-trapped solutions but we believe that the dynamics of filaments studied in [28] and elaborated below can provide valuable physical insight and reflects key features underlying evolution from more general initial conditions. This conclusion is supported by similarities between the numerical simulations of Torner and Petrov [32] in which they observed breakup in quadratic nonlinear media of input Laguerre-Gaussian modes with phase dislocation, and the evolution of the corresponding self-trapped solutions; see below and [23,28].

Note that the solutions discussed above are assumed to be linearly polarized in the transverse plane. For the Maxwell equations for a purely azimuthal field propagating in Kerr-like media the existence of a family of many-ring solutions with a dark central spot [33] and its azimuthal instability [34] have been reported. The model equation studied is like the NLS, but with an additional term of the form r^{-2} (r is the radial coordinate) argumenting the usual transverse Laplacian operator. This model has some formal resemblance to the case of a scalar field with a singly charged vortex, but the analogy has not been developed by these authors, and we will not pursue it here.

This paper is an expansion and extension of development of our initial work [28], and is organized as follows. The next two sections are devoted to a detailed stability analysis of one- and two-ring stationary solitary waves with phase dislocations, analyzing both saturable and quadratic nonlinear media. All these waves are propagation-unstable, breaking up into filaments, and the physically interesting features lie in the mechanism of filamentation, and the dynamics of the daughter filaments. By varying relevant parameters over a wide range, we demonstrate transitions between different filamentation scenarios, and a rich variety of output patterns. We anticipate that input beams that are in some sense close to these higher-order solitons will show the same classes of filamantation behavior. In the last section we develop an analytical approach to the study of filament dynamics after the breakup. We derive two different analytical expressions for the velocity of the filaments in the transverse plane. One is based on the conservation of the angular momentum, while the other is derived using the conservation of the Hamiltonian. Both formulas give reasonably good quantitative predictions for the velocities, the formula based on angular momentum being particularly effective. Both formulas give important insight into the underlying physics of the beam breakup. The stability analysis and analytical results are complemented by an extensive series of numerical simulations of the original models, which verifies their predictions and gives detailed quantitative information on the evolution of beams carrying angular momentum in nonlinear optical media.

II. SELF-TRAPPED BEAMS WITH PHASE DISLOCATION IN SATURABLE MEDIA

A. Model and stationary solutions

The evolution of the slowly varying electric field envelope $\mathcal{E}$ in the nonlinear media is governed by the equation (see, e.g., [30])

$$2ik\partial_Z\mathcal{E}+\partial_X^2\mathcal{E}+\partial_Y^2\mathcal{E}+2k\frac{\omega_0}{c}n_{\mathrm{NL}}(I)\mathcal{E}=0, \tag{1}$$

Z and X,Y are the longitudinal and transverse coordinates, ω_0 is the carrier frequency, $k=n_0\omega_0/c$ is the carrier wave number in the medium, n_0 is the (linear) refractive index, and c the velocity of light in vacuum. The field is scaled such that $I=|\mathcal{E}|^2$ is the intensity, and $n_{\mathrm{NL}}(I)$ is the intensity dependent part of the refractive index. The form of n_{NL} depends on the medium: e.g., for a Kerr medium $n_{\mathrm{NL}}=n_2I$. In most media the index change shows some form of saturation. For example, in a two-level medium excited well off resonance the nonlinear index can be described by $n_{\mathrm{NL}}=n_2I/(1+I/I_{\mathrm{sat}})$, with I_{sat} the saturation intensity. This is the model we will use in the present paper. Such a medium is self-focusing $n_2>0$ (or more generally $dn_{\mathrm{NL}}/dI>0$) and self-defocusing in the opposite situation.

We now rescale our variables so as to reduce Eq. (1) to the dimensionless form

$$i\partial_zE+\tfrac{1}{2}\vec{\nabla}_\perp^2E+f(|E|^2)E=0 \tag{2}$$

through the following substitutions: $Z=zl_d$, $X=wx$, $Y=wy$, $\mathcal{E}=E\sqrt{I_{\mathrm{sat}}l_{\mathrm{nl}}/l_d}$, where $l_d=kw^2$ and $l_{\mathrm{nl}}=c/(\omega_0|n_2|I_{\mathrm{sat}})$ are the diffraction and nonlinear lengths, w is a characteristic transverse length scale, $\vec{\nabla}_\perp=\vec{i}\partial_x+\vec{j}\partial_y$. We will concentrate henceforth on the model of the self-focusing saturable nonlinearity

$$f(|E|^2)=\frac{|E|^2}{1+\alpha|E|^2},\quad \alpha=\frac{l_{\mathrm{nl}}}{l_d}, \tag{3}$$

Here α is a saturation parameter, and clearly the Kerr limit is simply given by $\alpha=0$. For this reason, and also for computational convenience, we retain α as a scaling parameter, even though it can clearly be scaled away.

It is well known, and qualitatively clear, that under an appropriate balance between diffractive stretching and nonlinear focusing ($l_d\sim l_{\mathrm{nl}}$) the electromagnetic radiation can be self-trapped forming a self-induced waveguide. Formally this means that Eq. (2) has nondiffracting solutions of the form

$$E(x,y,z)=\mathcal{A}(x,y)e^{i\kappa z}. \tag{4}$$

Here κ has a sense of the eigenvalue of the corresponding waveguide mode, which many authors term as the nonlinear wave-vector shift. The transverse profile $\mathcal{A}(x,y)$ obeys

$$\vec{\nabla}_\perp^2\mathcal{A}=2[\kappa-f(|\mathcal{A}|^2)]\mathcal{A}. \tag{5}$$

Beam confinement demands exponential decay of $|\mathcal{A}|$ at infinity, which requires $\kappa>0$. Multiplying Eq. (5) by $\mathcal{A}^*$ and integrating the left-side by parts one gets

$$-\int dxdy|\vec{\nabla}_\perp\mathcal{A}|^2=\int dxdy[\kappa-f(|\mathcal{A}|^2)]|\mathcal{A}|^2 > (\kappa-\max f)\int dxdy|\mathcal{A}|^2. \tag{6}$$

Since $f<\alpha^{-1}$, any self-trapped solutions of our model must have $0<\kappa<\alpha^{-1}$.

Below we will concentrate on one particular class of self-trapped solutions of Eq. (5) namely, those with a phase singularity at the center, which have the form

$$\mathcal{A}(x,y)=A(r)e^{il\theta}, \tag{7}$$

where $r=\sqrt{x^2+y^2}$, θ is the polar angle, and $A(r)$ is the real function obeying

$$\frac{d^2A}{dr^2}+\frac{1}{r}\frac{dA}{dr}-\frac{l^2}{r^2}A=2[\kappa-f(A^2)]A, \tag{8}$$

Physically l must be an integer (there is no phase singularity for $l=0$), while $A(r)$ must obey the following boundary conditions:

$$r\to 0,\quad A(r)\to r^{|l|}c_0, \qquad r\to\infty,\quad A(r)\to\frac{c_\infty}{\sqrt{r}}e^{-r\sqrt{2\kappa}}, \tag{9}$$

where $c_{0,\infty}$ are real constants. There is redundancy in Eq. (8), since either κ or α can be scaled away. We prefer to keep them both: α to provide transition to the pure cubic nonlinearity and κ to retain the traditional form of the Vakhitov-Kolokolov stability criterion [20] (for more details see next subsection).

Equation (8) with boundary conditions (9) were solved numerically using a second-order finite difference method. We found that for any nonzero integer l one-, two- and many-ring solutions with a central phase singularity exist in the entire region $0<\kappa<\alpha^{-1}$; see above and [35]. Typical radial profiles of A for different values of l are presented in Fig. 1. While these profiles can obviously be approximated by analytical techniques (see, e.g., [14,27]) here we confine ourselves to numerical solutions, which have, in principle, arbitrarily high accuracy.

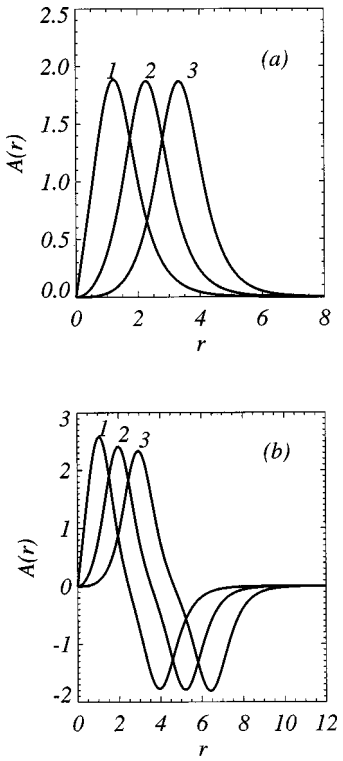

FIG. 1. Plots of the field amplitude $A(r)$ for $l=1,2,3$, $\kappa=1$, and $\alpha=0.1$. (a) One-ring and (b) two-ring solutions of Eq. (8). The labels in Figs. 1, 2 denote l values.

B. Stability

Having found these stationary solutions, their stability is a natural question to study. Consider small complex perturbations $\varepsilon(z,r,\theta)$ of the stationary solution (7),

$$E(z,r,\theta)=[A(r)+\varepsilon(z,r,\theta)]e^{i\kappa z+il\theta}. \tag{10}$$

The general solution of the linearized problem for ε can be expressed as a superposition of azimuthal Fourier modes $e^{\pm iJ\theta}$ $(J=0,1,2,\dots)$ with complex coefficients dependent on r and z. Therefore looking for the exponentially growing perturbations that characterize instability, we set

$$\varepsilon(z,r,\theta)=g_J^+(r)e^{\lambda_J z+iJ\theta}+g_J^-{}^*(r)e^{\lambda_J^* z-iJ\theta} \tag{11}$$

and obtain the following non-self-adjoint eigenvalue problem:

$$i\lambda_J\vec{g}_J=\begin{bmatrix}\hat{L}_J^+ & A^2f'\\ -A^2f' & -\hat{L}_J^-\end{bmatrix}\vec{g}_J, \tag{12}$$

where $\vec{g}_J=(g_J^+,g_J^-)^T$, $f'=df/dA^2$, and

$$\hat{L}_J^\pm=\frac{1}{2}\left[\frac{1}{r}\frac{d}{dr}r\frac{d}{dr}-\frac{1}{r^2}(l\pm J)^2\right]-\kappa+f+A^2f'.$$

Note that Eq. (12) is obviously valid for $l=0$, i.e., for the solitary waves with finite intensity at $r=0$. It can be shown that for $l=0$ perturbations proportional to $\cos J\theta$ and $\sin J\theta$ are equivalent and can be treated independently. This fact was implicitly used in Refs. [21,34]. Therefore the dimen-

sion of the eigenvalue problem in the space of real functions can be reduced from 4×4 to 2×2 when $l=0$. This also follows from the fact that if $l=0$ then Eq. (12) has the solutions $g_J^- = \pm g_J^{+*}$. The presence of a phase singularity destroys this symmetry property and cosine and sine perturbations cannot be decoupled.

The asymptotic behavior of the eigenvectors $\vec{g}_J$ is

$$r\to 0, \quad g_J^{\pm}(r)\to r^{|l\pm J|}b_0^{\pm},$$
$$r\to\infty, \quad g_J^{\pm}(r)\to\frac{b_\infty^{\pm}}{\sqrt{r}}e^{-r\sqrt{2(\kappa\pm i\lambda_J)}}, \tag{13}$$

where $b_{0,\infty}^{\pm}$ are complex constants and the branch of the square root in the exponent must be chosen such that the unstable eigenfunctions are square integrable. The eigenvalues of the discrete spectrum corresponding to such eigenfunctions can lie anywhere in the complex plane outside the rays $(i\kappa, i\infty)$ and $(-i\kappa, -i\infty)$, which belong to the continuous spectrum with extended eigenfunctions. Unstable eigenmodes have eigenvalues with $\mathrm{Re}\lambda_J>0$. They must always have a counterpart with $\mathrm{Re}\lambda_J<0$ because of the Hamiltonian nature of our problem; see Sec. IV.

Due to the phase ($E\to Ee^{i\phi}$) and translational [$E(x,y)\to E(x+\delta x, y+\delta y)$] symmetries of the our model Eq. (12) has neutrally stable modes for $J=0,1$, i.e., modes with zero eigenvalues. They are

$$\vec{g}_0^{(0)}=\begin{bmatrix} A \\ -A \end{bmatrix}, \quad \vec{g}_1^{(0)}=\begin{bmatrix} \dfrac{dA}{dr}-\dfrac{l}{r}A \\ \dfrac{dA}{dr}+\dfrac{l}{r}A \end{bmatrix}. \tag{14}$$

Neutral modes are important for analytic approaches to stability problems of this type. Asymptotic techniques (see, e.g., [8]) can be used to show that the neutrally stable mode $\vec{g}_0^{(0)}$ branches at the point $\partial_\kappa Q=0$ giving instability of any bound solution of Eq. (8) if

$$\partial_\kappa Q<0; \tag{15}$$

here Q is the energy flux

$$Q=\int dxdy|E|^2. \tag{16}$$

Thus the standard stability criterion for the ground states [20] is also a *necessary* condition for the stability of self-trapped beams with a phase dislocation.

For pure Kerr media ($\alpha=0$) $\partial_\kappa Q=0$ and a collapse instability is present [25]. The evolution of this collapse in z is of polynomial type, therefore it can easily be suppressed by an exponential instability if there is one. This is indeed the case in our situation due to the exponential instabilities for $J\neq0$ described below. In case of single-ring solutions with $l\neq0$, which have no nodes for $r>0$, a variational approach to the eigenvalue problem (12) can be applied in a manner similar to that done in Refs. [20,34]. It shows that $\partial_\kappa Q>0$ is also *sufficient* for stability against *symmetry-preserving* perturbations ($J=0$). Plots of the energy vs κ for the one-ring solutions are presented in Fig. 2. We conclude that the one-ring solitary waves are stable with respect to $J=0$ perturbations in the saturable media. For many-ring solutions there is no comparable approach, nor any simple criterion that is sufficient for symmetry-preserving stability and numerical checks are always necessary.

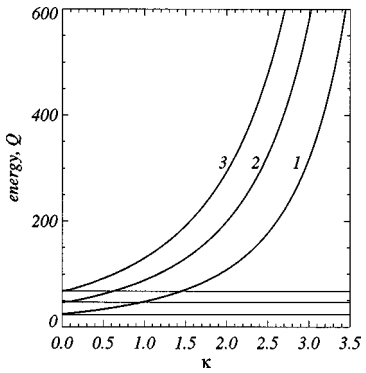

FIG. 2. Energy Q vs κ for one-ring solutions with $l=1,2,3$ and $\alpha=0.2$. Horizontal lines correspond to a pure Kerr medium, $\alpha=0$.

The above analytic criterion says nothing about stability against *symmetry breaking* perturbations, i.e., MI is not excluded even where $\partial_\kappa Q>0$ holds. Azimuthal MI corresponds to modes with $J\neq0$ having exponential growth, in general leading to J-fold intensity modulation around the ring, breaking the cylindrical symmetry of the intensity of the stationary solution. For $J=1$ we might hope for an analytic result linked to the $g_1^{(0)}$ neutral mode, but asymptotic expansion shows that this neutral mode is not linked to the

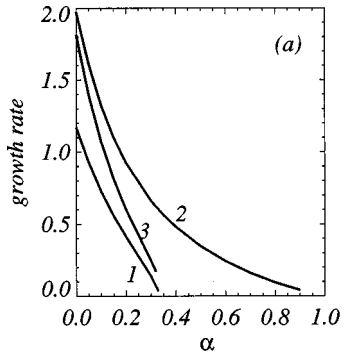

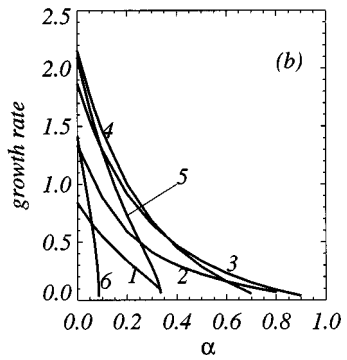

FIG. 3. Growth rates of the unstable eigenmodes of the one-ring solution vs α for $\kappa=1$. (a) $l=1$, (b) $l=2$. Here and in Figs. 4, 8, 13, 15 numbers denote J values.

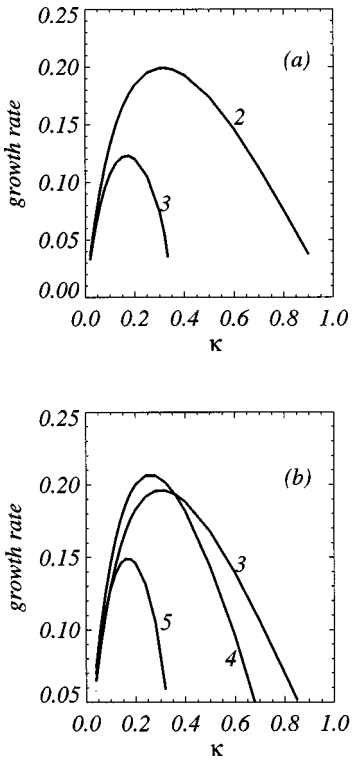

FIG. 4. Growth rates vs κ of the most unstable eigenmodes of the one-ring solution for $\alpha=1$. (a) $l=1$, (b) $l=2$.

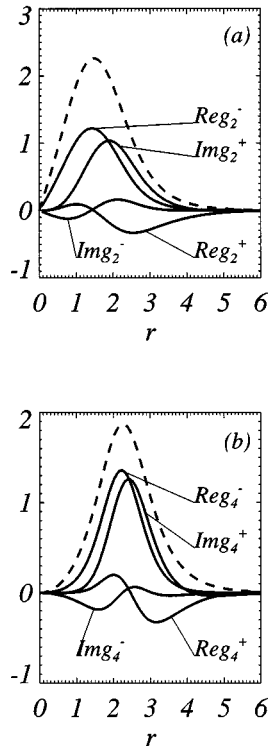

FIG. 5. Real and imaginary parts of the maximally unstable eigenmodes for one-ring solutions. (a) $l=1$, $J=2$, $\alpha=0.3$, $\kappa=1$ and (b) $l=2$, $J=4$, $\alpha=0.1$, $\kappa=1$. Dashed lines mark the radial profile of the self-trapped solution $A(r)$.

appearance of any instability. However, this obviously does not forbid the presence of instability for any $J\neq 0$ including $J=1$ and we are obliged to study the eigenvalue problem (12) with a different method. There are several possible numerical approaches to solve such problems; see, e.g., [21,36,37]. We chose to reduce Eq. (12) to an algebraic eigenvalue problem by replacing the differential operators with the second-order finite differences. We apply zero boundary conditions for some large value of r and appropriate conditions at $r=0$, as given in Eq. (13). 200 to 300 grid points was usually enough to get good precision. Zero boundary conditions for large r is a potential source of problems because weakly decaying eigenvectors require large numbers of grid points to maintain accuracy. However, we did not meet such a situation in any of the investigations described in this paper. Furthermore, numerical results for the neutrally stable modes were always in good agreement with Eqs. (14).

Numerical analysis of symmetry-breaking perturbations ($J\neq 0$) shows the presence of instabilities over a finite range of values of J in every case. The results for the one-ring solutions with $l=1,2,3$, $\kappa=1$ and $\alpha=0.1$ were presented earlier in Ref. [28]. Here we study in detail how variations of the parameters and of the initial noise level influence symmetry-breaking instabilities of the one-ring solitary waves with $l=1,2$ and two-ring wave with $l=1$. These cases are typical of the breakup of ring stationary waves in saturable Kerr media that carry orbital angular momentum.

Let us first describe the one-ring solutions. Although, because of the above-mentioned scaling, all possible situations can in fact be captured by varying just one parameter and keeping the other fixed, for convenience and ease of interpretation we plot the growth rates ($\mathrm{Re}\lambda_J$) of the unstable eigenmodes versus both parameters; see Figs. 3 and 4. For $l=1$ just three unstable eigenmodes ($J=1,2,3$) appear, with the $J=2$ mode dominating through the whole range of α and κ. For $l=2$ either of the two modes $J=3,4$ can be dominant depending on the parameter values. Generally the instability gets stronger for $\alpha\to 0$ and it is practically suppressed for $\alpha\to 1/\kappa$. Suppression of MI (of any nature) with increasing saturation is a common phenomenon that has also been reported for the fundamental bright and dark solitons in saturable media [5,37]. Considering variations of κ, for κ close to 0 or to $1/\alpha$ the instability is again practically suppressed. This is also typical for the symmetry-breaking instabilities of other kinds of the ring structures [21,27,34].

We found that the unstable eigenvalues are generally complex. If the instability for an eigenmode disappears within the existence region of the solitary solution the imaginary part of the corresponding λ_J usually remains finite as its real part vanishes. In particular this holds for the unstable eigenmode with $J=1$, and it explains why instability for this mode cannot be captured by asymptotic expansion near the neutral mode $\vec{g}_1^{(0)}$.

We found that the radial profiles of the most unstable eigenfunctions mainly concentrate around the rings of the stationary solutions; see Fig. 5. Because $A(r)$ is real, it is the real part of the perturbations that determines the field amplitude modulation pattern that develops around an unstable ring. Therefore we expect the initially uniform ring will develop $J_{\max}$ minima and $J_{\max}$ maxima on propagation, where $J_{\max}$ is the azimuthal index of the perturbation eigenmode with the maximal growth rate. As a consequence, the ring should break up into $J_{\max}$ filaments. However, other eigenmodes, in particular those with $J=J_{\max}\pm 1$, can have com-

parable growth rates, which can affect the filamentation process and make the output pattern depend somewhat on the particular realization of the initial noise.

To test the results of our stability analysis we performed an extensive series of numerical simulations of Eq. (2) with initial conditions in the form

$$E(r,\theta)=\{1+s[q_r(r,\theta)+iq_i(r,\theta)]\}A(r)e^{il\theta}, \quad (17)$$

where $q_{r,i}$ are real functions modeling Gaussian noise in the interval $(-1,1)$ and s is a constant. Simulation was done on the polar grid with 128 and $200-300$ grid points along the angular and radial coordinates, respectively. The polar grid prevents the numerical noise effects of discretizing a ring onto a rectangular grid from unduly influencing the number of filaments formed. For low noise level (s of the order 0.01 or less) the most unstable eigenmode was clearly dominant in the majority of simulations. Increasing the noise to $s \sim 0.1$ led to the occasional appearance of $J=J_{\max}\pm 1$ filaments. In most of the simulations the filaments formed from the same ring had similar intensities. This suggests that the unstable eigenmode dominating at the beginning of the instability suppresses all the others. [For an exception see Fig. 6(b).]

Examples of the breakup of one-ring solutions with $l=1$ into 2 and 3 filaments and with $l=2$ into 4, 5, and 3 filaments are presented in Figs. 6 and 7. Parameters and level of the initial noise are specified in the figure captions. There is excellent agreement between the predictions of the stability analysis (see Fig. 3) and the results of these direct numerical simulation of the original model.

In the case of a pure Kerr medium ($\alpha=0$) the exponential growth of the symmetry-breaking perturbations should dominate over the algebraic growth of the symmetry-preserving collapse instability. In the simulations for the Kerr case we indeed first observed filamentation of the ring and subsequently collapse of the filaments.

For the two-ring solitary solutions with $l=1$, we present just the growth rates for the dominant eigenmodes versus α; see Fig. 8. All unstable eigenmodes can be naturally separated into two groups. The radial profiles of the eigenmodes from one group concentrate around the first ring and from the other around the second ring; see Fig. 9. Because of this each ring develops its own modulated pattern and breaks up into the different number of filaments. We present here (see Fig. 10) results of numerical simulation for $\alpha=0.05$ (when $J=2$ and $J=6$ modes dominate for the first and second ring, respectively) and for $\alpha=0.6$ with dominant $J=2$ and $J=5$ modes. For $\alpha=0.05$ the first ring is more unstable and for $\alpha=0.6$ the second ring is more unstable. For the latter situation the instability of the first ring is so weak that its breakup did not occur within the propagation distance simulated.

The examples presented in Figs. 6, 7 and 10 show that filamentation happens over propagation distances from several to several tens of diffraction lengths. For small values of α and optimal initial energy, i.e., adjusting κ to maximize the instability, we were able to observe filamentation within one or two diffraction lengths.

Finally, regarding the possibility of analytical study of the stability with respect to symmetry-breaking perturbations we suggest that a proper generalization of the averaging techniques described in [21] may be the most efficient way to do it.

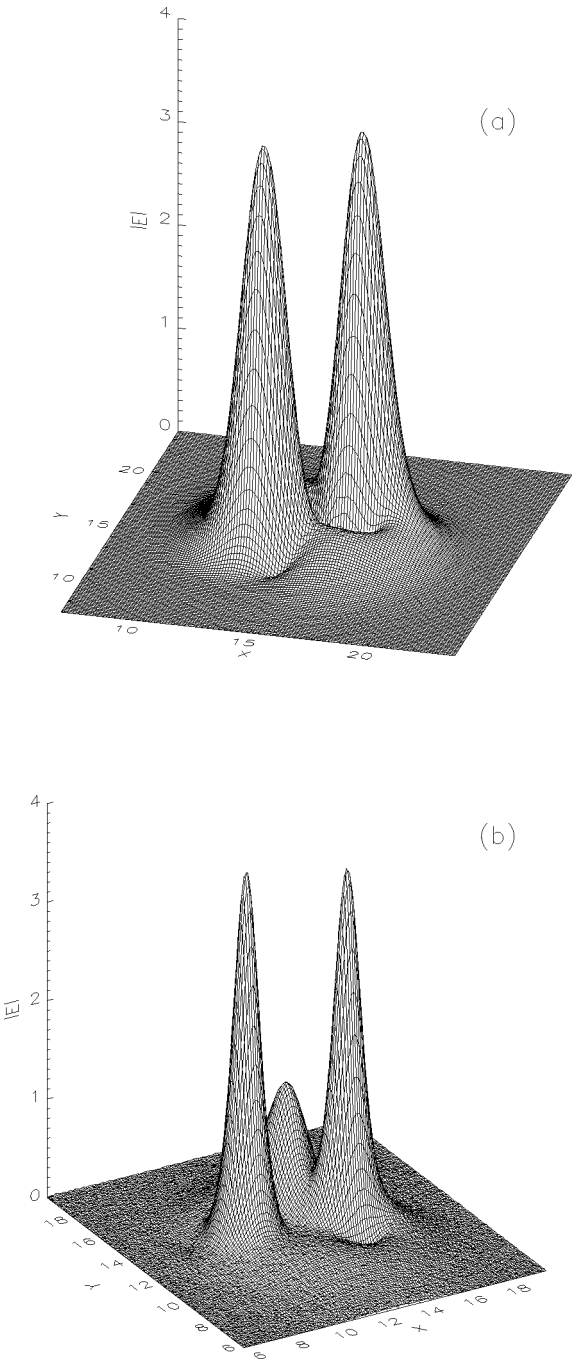

FIG. 6. Breakup of the one-ring solution with $l=1$, $\kappa=1$. (a) $\alpha=0.3$, $s=0.01$, $z=14$; (b) $\alpha=0.1$, $s=0.05$, $z=7$.

III. SELF-TRAPPED BEAMS WITH PHASE DISLOCATION IN QUADRATIC MEDIA

The main qualitative features of the dynamics in quadratic media of self-trapped beams with phase dislocation are the same as in saturable media [28]. The latter model was elaborated in some detail in the previous section. In addition, stability in the ''quadratic case'' has been investigated not only by us [28] but also by Torres *et al.* [23]. Therefore in this

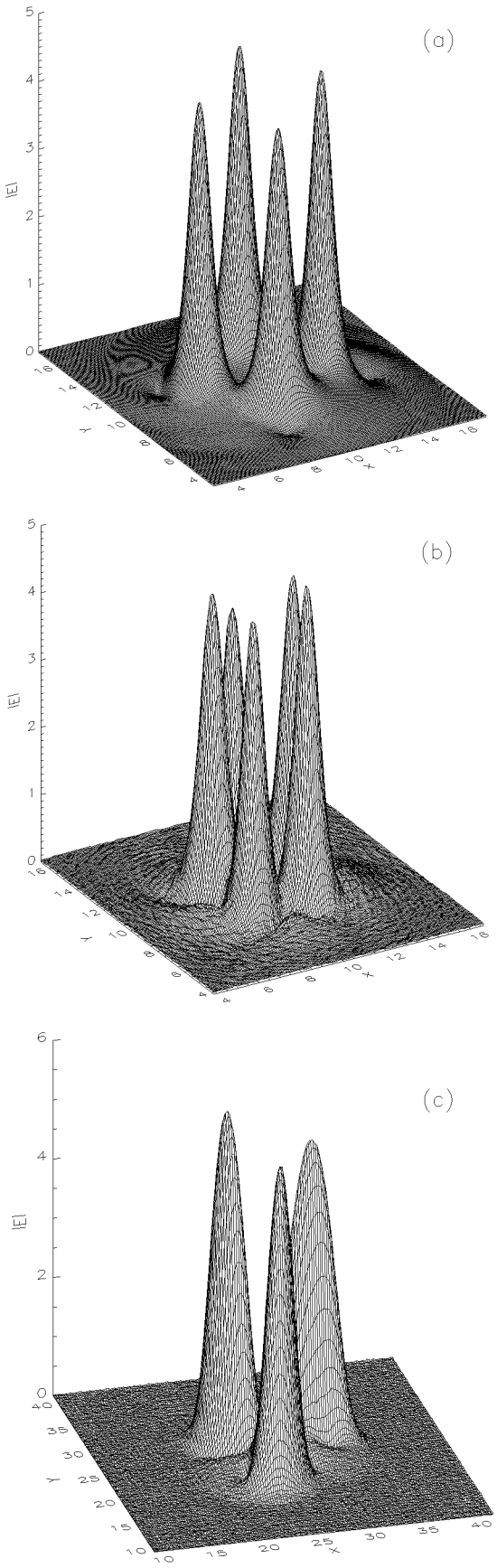

FIG. 7. Breakup of the one-ring solution with $l=2$, $\kappa=1$. (a) $\alpha=0.1$, $s=0.005$, $z=7$; (b) $\alpha=0.1$, $s=0.08$, $z=4$; (c) $\alpha=0.6$, $s=0.08$, $z=26$.

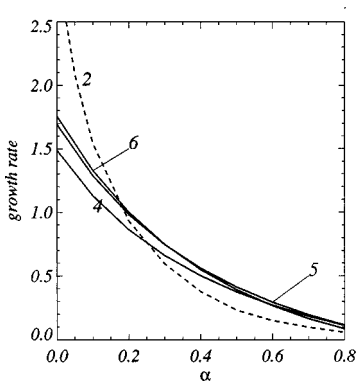

FIG. 8. Growth rates of selected unstable eigenmodes of the two-ring solution vs α for $\kappa=1$ and $l=1$. Dashed (full) lines are for the modes concentrated around the first (second) ring.

section we will present our results in somewhat compressed form, concentrating on gaps in the previous treatments and on differences from the saturable case.

A. Model and stationary solutions

The evolution of the slowly varying envelopes of the fundamental ($\mathcal{E}_1$) and second harmonic ($\mathcal{E}_2$) electric fields in a noncentrosymmetric crystal is governed by the following equations (see, e.g., [7]):

$$2ik_1\partial_Z\mathcal{E}_1+\partial_X^2\mathcal{E}_1+\partial_Y^2\mathcal{E}_1+\frac{\omega_0^2}{c^2}\chi_1\mathcal{E}_1^*\mathcal{E}_2e^{-i\delta kZ}=0,$$

$$2ik_2\partial_Z\mathcal{E}_2+\partial_X^2\mathcal{E}_2+\partial_Y^2\mathcal{E}_2+4\frac{\omega_0^2}{c^2}\chi_2\mathcal{E}_1^2e^{i\delta kZ}=0, \tag{18}$$

where ω_0 is the carrier frequency of the fundamental wave, $k_1=k_1(\omega_0)$ and $k_2=k_2(2\omega_0)$ are the wave vectors in the medium, $\delta k=2k_1-k_2$, $\chi_{1,2}$ are proprtional to the relevant elements of the nonlinear susceptibility tensor.

We reduce Eqs. (18) to dimensionless form

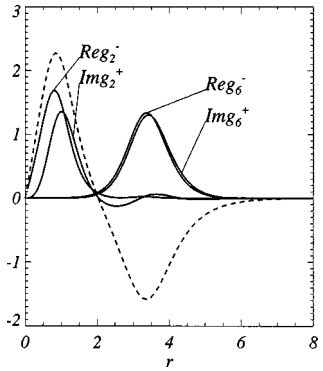

FIG. 9. Real and imaginary parts of the maximally unstable eigenmodes for the two-ring solution. $l=1$, $\alpha=0.05$, $\kappa=1$. $J=2$ and $J=6$ for the eigenmodes concentrated around the first and second ring, respectively. Dashed line: radial profile of the self-trapped solution $A(r)$.

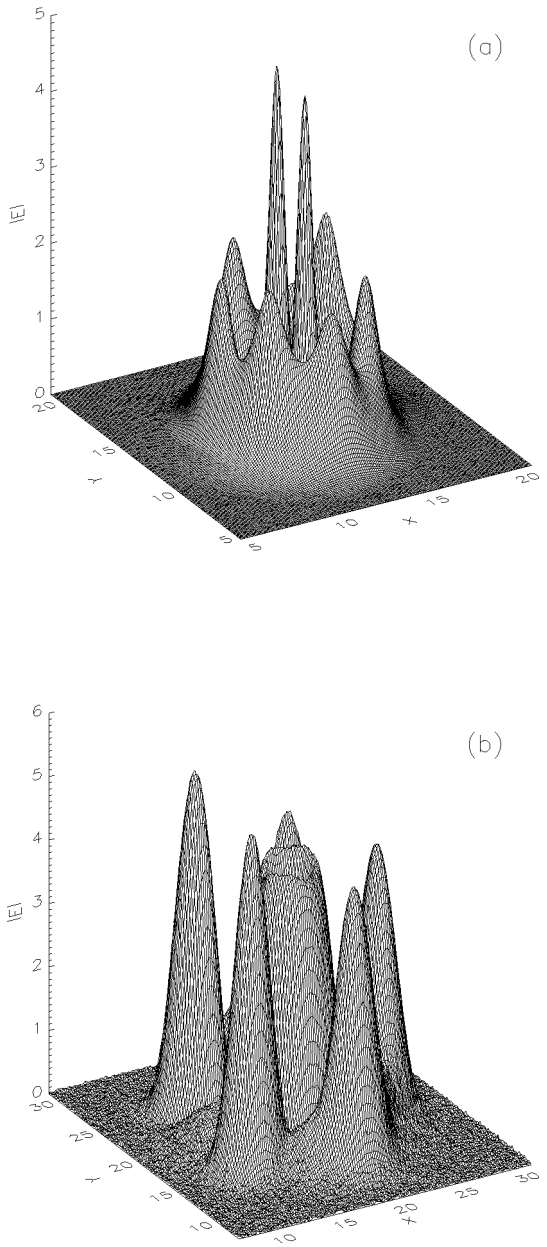

FIG. 10. Breakup of the two-ring solution with $l=1$ and $\kappa=1$. (a) $\alpha=0.05$, $s=0.005$, $z=4$; (b) $\alpha=0.6$, $s=0.1$, $z=26$.

$$\partial_z E_1+\tfrac{1}{2}\vec{\nabla}_\perp^2 E_1+E_1^* E_2=0,$$
$$\partial_z E_2+\tfrac{1}{4}\vec{\nabla}_\perp^2 E_2+\frac{1}{2}E_1^2=\beta E_2, \tag{19}$$

through the following substitutions: $Z=l_d z$, $X=wx$, $Y=wy$, $\mathcal{E}_1=E_1 k_1 c/(l_d\omega_0^2\sqrt{\chi_1\chi_2})$, $\mathcal{E}_2=E_2 e^{i\beta z}2k_1c^2/(l_d\omega_0^2\chi_1)$, where $l_d=k_1w^2$ is the diffraction length, $\beta=\delta k l_d$ is the phase mismatch parameter. We neglected spatial walk-off effects, thereby implicitly supposing that the walk-off length is the longest characteristic length in the problem. We also made the natural choice $k_2/k_1=2$ in Eq. (19).

We look for stationary solutions of Eqs. (19) in the form

$$E_m=A_m(r)e^{im(l\theta+\kappa z)}, \quad m=1,2. \tag{20}$$

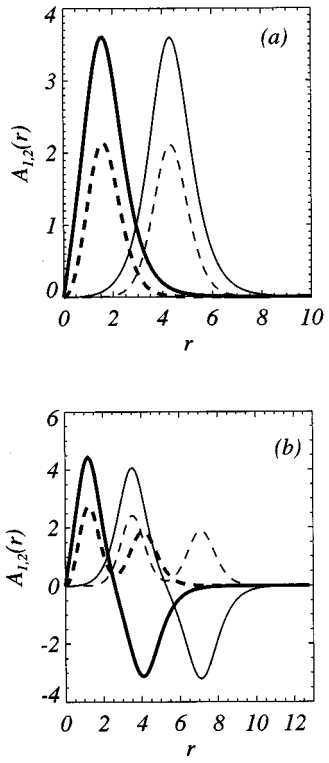

FIG. 11. Plots of the field amplitudes $A_1(r)$ (full lines) and $A_2(r)$ (dashed lines) of (a) one-ring and (b) two-ring solutions of Eq. (21) for $l=1$ (thick lines), $l=3$ (thin lines). $\kappa=1$ and $\beta=0$.

The real amplitudes $A_{1,2}$ obey the equations

$$\frac{d^2A_1}{dr^2}+\frac{1}{r}\frac{dA_1}{dr}-\frac{l^2}{r^2}A_1=2(\kappa-A_2)A_1,$$
$$\frac{d^2A_2}{dr^2}+\frac{1}{r}\frac{dA_2}{dr}-\frac{4l^2}{r^2}A_2=4(2\kappa+\beta)A_2-2A_1^2. \tag{21}$$

Equations (21) have a family of ringlike solutions similar to the case of the saturable medium. However, there is no condition similar to Eq. (6) and therefore just the requirement of exponential decay of the tails imposes a restriction on the parameter range where the solitary solutions can exist, namely, $\kappa>\max(0,-\beta/2)$. Radial profiles of $A_{1,2}$ for one- and two-ring cases are presented in Fig. 11. For the many-ring solutions the fundamental field A_1 has radial nodes but the second harmonic A_2 always remains positive, though having minima close to the zeros of the fundamental. For large β Eqs. (19) can be approximately reduced to the NLS equation for the fundamental field [6], and for increasing β the second harmonic tends to carry less and less of the total energy. A_2 goes to zero faster than A_1 as $r\to0$ because the order of the phase singularity for the second harmonic is double that of the fundamental one.

One of the parameters κ or β can be scaled away from Eqs. (21). However, we like to keep them both: β is not a very natural parameter for scaling because it can be positive, negative, or zero and we keep κ because of its physical in-

terpretation as a nonlinear wave vector correction, and also, as remarked above, because it is the natural parameter for investigation of stability.

B. Stability

The weaker character of the nonlinearity compared with the Kerr case means there is no collapse in quadratic media, and instabilities are associated with exponential growth of perturbations. Considering small perturbations of the stationary solutions (20) in the form

$$\epsilon_m(z,r,\theta)=g_{Jm}^{+}(r)e^{\lambda_J z+iJ\theta}+g_{Jm}^{-}{}^{*}(r)e^{\lambda_J^{*}z-iJ\theta},\quad m=1,2 \tag{22}$$

we get the following non-self-adjoint eigenvalue problem

$$i\lambda_J\vec{g}_J=\begin{bmatrix}\hat{L}_{J1}^{+} & A_2 & A_1 & 0\\ -A_2 & -\hat{L}_{J1}^{-} & 0 & -A_1\\ A_1 & 0 & \hat{L}_{J2}^{+} & 0\\ 0 & -A_1 & 0 & -\hat{L}_{J2}^{-}\end{bmatrix}\vec{g}_J, \tag{23}$$

where $\vec{g}_J=(g_{J1}^{+},g_{J1}^{-},g_{J2}^{+},g_{J2}^{-})^T$ and

$$\hat{L}_{J1}^{\pm}=\frac{1}{2}\left[\frac{1}{r}\frac{d}{dr}r\frac{d}{dr}-\frac{1}{r^2}(l\pm J)^2\right]-\kappa,$$

$$\hat{L}_{J2}^{\pm}=\frac{1}{4}\left[\frac{1}{r}\frac{d}{dr}r\frac{d}{dr}-\frac{1}{r^2}(2l\pm J)^2\right]-2\kappa-\beta.$$

Pure imaginary λ_J belonging to the continuous spectrum lie in the rays $(i\Omega_c,i\infty)$ and $(-i\Omega_c,-i\infty)$, where $\Omega_c=\min(\kappa,2\kappa+\beta)$. Neutrally stable eigenmodes for $J=0$ and $J=1$ are

$$\vec{g}_0^{(0)}=\begin{bmatrix}A_1\\ -A_1\\ 2A_2\\ -2A_2\end{bmatrix},\quad \vec{g}_1^{(0)}=\begin{bmatrix}\dfrac{dA_1}{dr}-\dfrac{l}{r}A_1\\ \dfrac{dA_1}{dr}+\dfrac{l}{r}A_1\\ \dfrac{dA_2}{dr}-\dfrac{2l}{r}A_2\\ \dfrac{dA_2}{dr}+\dfrac{2l}{r}A_2\end{bmatrix}. \tag{24}$$

Symmetry-preserving $(J=0)$ perturbations of the one-ring solutions are damped for

$$\partial_\kappa Q=\partial_\kappa\int dxdy(|E_1|^2+2|E_2|^2)>0, \tag{25}$$

where Q is the energy flux. Representative plots of Q vs κ are presented in Fig. 12. The instability for negative β is related to the existence for $\partial_\kappa Q>0$ of a pair of the eigenmodes with purely imaginary eigenvalues (with opposite signs) lying in the gap $(-i\Omega_c,i\Omega_c)$. At the point $\partial_\kappa Q=0$ these eigenmodes coincide with the neutral mode $\vec{g}_0^{(0)}$ and for larger $|\beta|$ appear again but with real eigenvalues of opposite signs. For the one-ring solitary solution this is the only route to a symmetry-preserving instability. We found that it is always suppressed by stronger symmetry-breaking instabilities; i.e., MI is always dominant in this case.

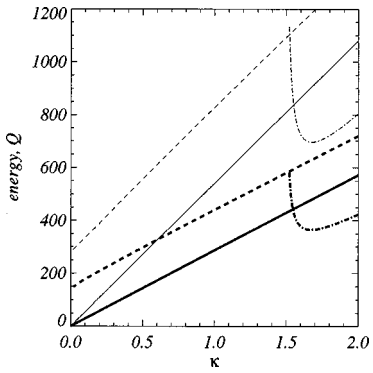

FIG. 12. Energy Q vs κ for one-ring solutions with $l=1$ (thick lines) and $l=2$ (thin lines): $\beta=-3$ (dash-dotted lines), $\beta=0$ (full lines), and $\beta=3$ (dashed lines).

For cases where $A_1(r)$ changes its sign (i.e., two or more rings), the criterion (25) is just a necessary condition and we found a new scenario of symmetry-preserving instability. It appears in a manner similar to that which we have described for solutions with a bright central spot and one or more rings [24]. However, we found that this instability may dominate the symmetry-breaking one only in a very narrow range of β values, close to the boundary of the solitary wave existence ($\beta<-1.9$ for $\kappa=1$). This contrasts with the case described in Ref. [24] (zero angular momentum), where the symmetry-preserving scenario is a major factor for a significant region of β values.

Plots of the growth rates of the unstable eigenmodes versus β for the one-ring solutions with $l=1,2$ presented in Fig. 13. In the limit of $\beta\gg1$ the dominating mode is the same as the one in the saturable medium for small saturation values, i.e, for α close to 0. The growth rates of the dominating eigenmodes increase linearly with increasing κ; see Ref. [23]. An example of the radial profiles of the components of the most unstable eigenmode is presented in Fig. 14.

The growth rates of the most unstable eigenmodes versus β for the two-ring solution with $l=1$ are presented in Fig. 15. (These results are restricted to $\beta>-1.9$ because for increasingly negative β the many-ring solitary solutions become very wide and extra care is needed in the stability analysis.) Again the localization of the eigenmodes on the rings suggests that during propagation any ring will break up into $J_{\max}$ filaments, where $J_{\max}$ shows maximum gain on that particular ring.

These predictions of our stability analysis are fully supported by simulations of Eqs. (19) and our comments in the previous section about saturable media, e.g., about the influence of noise on the symmetry-breaking instabilities, are also valid in quadratic media. An example of the break up of the one-ring solution with $l=2$ to four filaments is presented in Fig. 16.

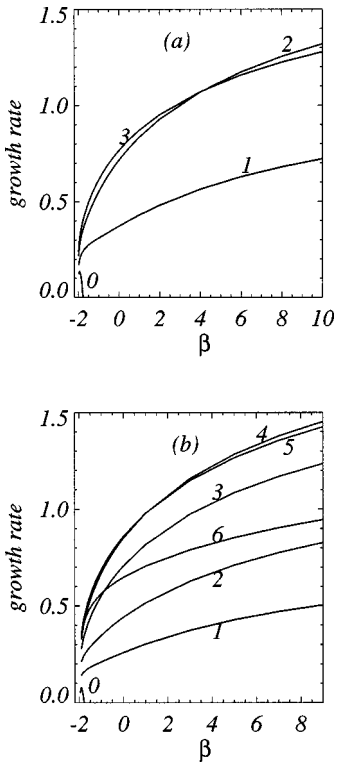

FIG. 13. Growth rates of the maximally unstable eigenmodes of the one-ring solution vs β for $\kappa=1$. (a) $l=1$, (b) $l=2$.

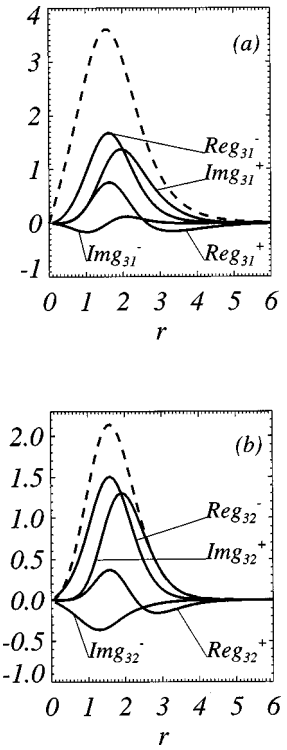

FIG. 14. Real and imaginary parts of the maximally unstable eigenmodes of the one-ring solution. $l=1$, $J=3$, $\beta=0$, $\kappa=1$. (a) is for the fundamental field and (b) is for the second harmonic. Dashed lines mark the radial profiles of the self-trapped solution, $A_{1,2}(r)$.

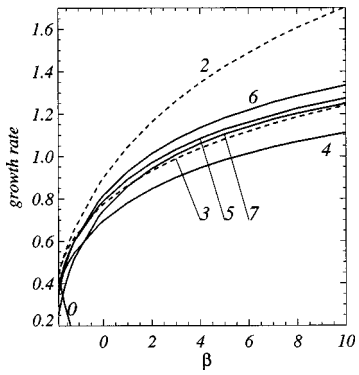

FIG. 15. Growth rates of selected unstable eigenmodes of the two-ring solution vs β for $\kappa=1$ and $l=1$. Dashed (full) lines are for the modes concentrated around first (second) ring.

IV. DYNAMICS OF FILAMENTS

As was shown above, self-trapped beams with a phase dislocation at the center and with varying numbers of rings exist as stationary solutions in both saturable and quadratic nonlinear media. They are unstable against symmetry-breaking perturbations, breaking up into a set of filaments during propagation. In this section we extend the analysis of the dynamics of the filaments outlined by us in [28]. This analysis is based on the conservation laws. Given initial values of the conserved quantities we show how to predict featues of the trajectories of the filaments, and even how to estimate their number.

The conserved Hamiltonian and momenta, which are essential to our present purposes, are introduced by a Lagrangian reformulation of the problems. This also makes it possible to develop analogies between solitary waves and particles.

Equations (19) can be written as Euler-Lagrange equations

$$\frac{\partial}{\partial z}\frac{\partial \mathcal{L}}{\partial(\partial_z E_m^*)}=\frac{\partial \mathcal{L}}{\partial E_m^*}-\sum_{i=x,y}\partial_i\frac{\partial \mathcal{L}}{\partial(\partial_i E_m^*)},\quad m=1,2, \tag{26}$$

where the Lagrangian density $\mathcal{L}$ is

$$\mathcal{L}=\frac{i}{2}\sum_{m=1,2}(E_m^*\partial_z E_m-\text{c.c.})-\mathcal{H}. \tag{27}$$

The corresponding formulas for Eq. (2) can be obtained by simply omitting the subscript m, and this procedure will be implied in most formulas below, exceptions being stated explicitly.

In the above, $\mathcal{H}$ is the corresponding Hamiltonian density, which for Eqs. (19) takes the form

$$\mathcal{H}=\tfrac{1}{2}|\vec{\nabla}_\perp E_1|^2+\tfrac{1}{4}|\vec{\nabla}_\perp E_2|^2+\beta|E_2|^2-\tfrac{1}{2}(E_1^2E_2^*+\text{c.c.}), \tag{28}$$

while for Eq. (2)

$$\mathcal{H}=\frac{1}{2}|\vec{\nabla}_\perp E|^2-\int_0^{|E|^2}du f(u). \tag{29}$$

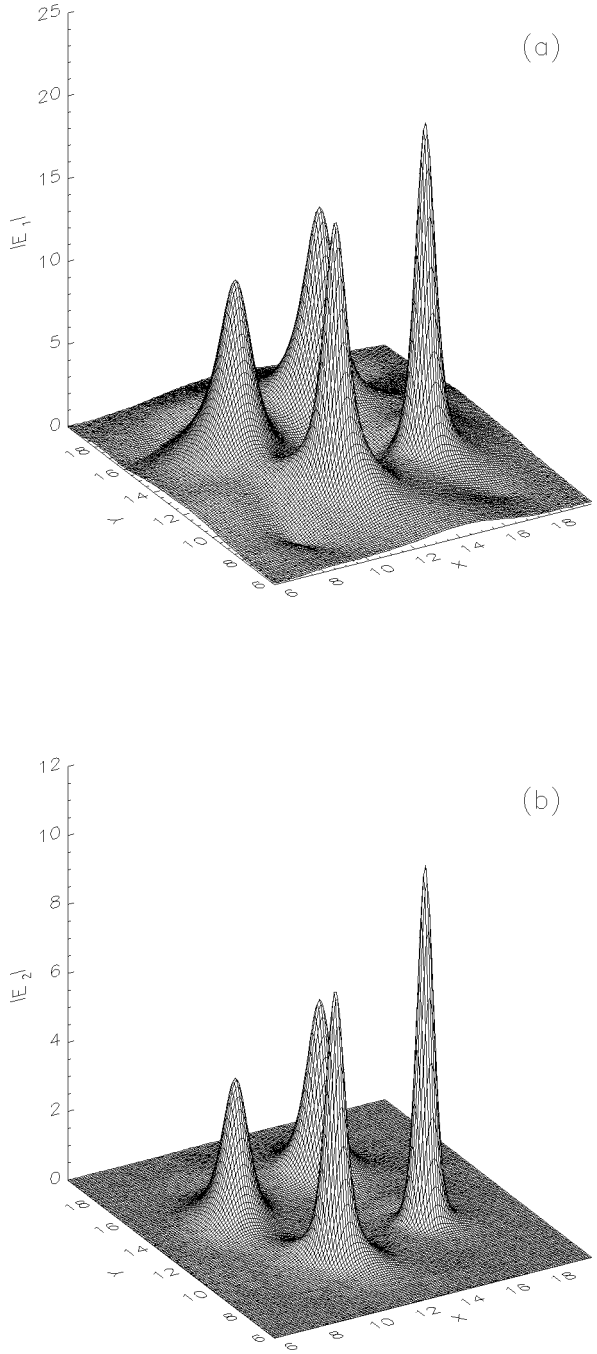

FIG. 16. Breakup of the one-ring solution with $l=2$, $\beta=5$, $\kappa=1$, $s=0.05$, $z=6$. (a) first harmonic, (b) second harmonic.

Considering variations of the action integral $S=\int_{z_1}^{z_2}dz\int dxdy\mathcal{L}$ with respect to infinitesimal spatial translations and rotations it can be shown that if $\mathcal{L}$ is invariant under these transformations the following two quantities are integrals of motion:

$$\vec{P}=\int dxdy\vec{\Pi}, \tag{30}$$

$$\vec{L}=\int dxdy\vec{r}\times\vec{\Pi}. \tag{31}$$

Here $\vec{r}=\vec{i}x+\vec{j}y$ and

$$\vec{\Pi}=-\sum_{m=1,2}\left(\frac{\partial\mathcal{L}}{\partial(\partial_z E_m)}\vec{\nabla}_\perp E_m+\text{c.c.}\right)$$

$$=\frac{1}{2i}\sum_{m=1,2}(E_m^*\vec{\nabla}_\perp E_m-\text{c.c.}). \tag{32}$$

By definition $\vec{P}$ is the linear momentum of the field, $\vec{L}$ its angular momentum, both expressed in terms of $\vec{\Pi}$, its linear momentum density. Solitary wave solutions (7), (20) carry zero linear momentum, $\vec{P}=0$, and nonzero angular momentum, $|\vec{L}|=|l|Q_0$, where Q_0 are the energy invariants [see Eqs. (16) and (25)], evaluated at these stationary solutions.

Equation (31) for the angular momentum is just the paraxial approximation for the optical orbital angular momentum per unit length [13]. The angular momentum carried by light beams has attracted much recent interest. It has been predicted, and proved experimentally, that Laguerre-Gaussian beams with azimuthal mode index l carry orbital angular momentum $l\hbar$ per photon [12]. Frequency doubling of such a beam has been shown [38] to generate a second harmonic with doubled azimuthal mode index $2l$.

Both our models (2), (19) have the property of Galilean invariance, e.g., in the quadratic medium:

$$(E_1,E_2,\vec{r})\rightarrow(E_1e^{i\Phi},E_2e^{2i\Phi},\vec{\xi}), \tag{33}$$

where

$$\Phi=\vec{v}(\vec{r}-\tfrac{1}{2}\vec{v}z),\quad \vec{\xi}=\vec{r}-\vec{v}z,\quad \vec{v}=\vec{i}v_x+\vec{j}v_y,$$

Under this transformation, a structure with zero linear momentum is boosted to $\vec{P}=Q\vec{v}$, therefore we can expect analogies with Newtonian mechanics with Q playing the role of mass. In particular, a fundamental soliton, which has no intrinsic angular momentum, will have orbital angular momentum $\vec{L}=\vec{r}\times Q\vec{v}$ about the origin, provided $|\vec{r}|$ is larger than the soliton size. It follows that if the total field can be regarded as a superposition of several separate localized structures, e.g., solitons, we can expect the dynamics of these structures (while they remain well localized) to be somewhat similar to the dynamics of mechanical particles.

For simulation of the soliton dynamics we used a split-step algorithm on a Cartesian grid with initial conditions obtained on the polar grid as described in Sec. II. Once the number of filaments is established the transition from one grid to the other does not cause any significant loss of precision. As a further check, conservation of energy, Hamiltonian, and momenta was monitored during the simulations.

We found numerically that filaments formed due to the azimuthal modulational instability do not diffract with propagation, but remain well localized and solitonlike. By superimposing images of the transverse intensity distribution at different z values we found that *these filaments move out along tangents to the initial ring, carrying away its orbital angular momentum*; see Fig. 17 for the case of a saturable medium. Several figures in Ref. [28] show this behavior for both saturable and quadratic media and different values of l.

Because, once fully formed, the filaments seem to behave like simple, *free* Newtonian particles, we now examine whether their number and dynamics can be predicted on the

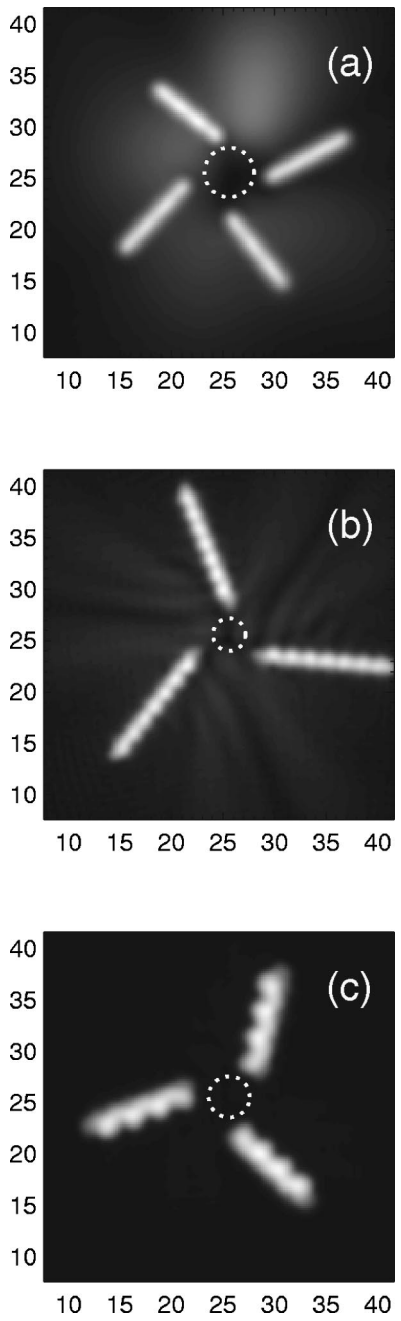

FIG. 17. Superimposed images of the transverse intensity distribution at different z values showing soliton trajectories in a saturable medium: $\alpha=0.1$, $l=2$. (a) $\kappa=1$, (b) $\kappa=5$, (c) $\kappa=8$. Propagation distance is $\Delta z=10$ for (a)–(c). Dotted lines mark the intensity maxima of the initial ring profiles.

basis of the quasimechanical considerations. We consider only the dynamics of the filaments formed after the breakup of the one-ring structures. This is because an essential condition to apply the ''mechanical'' approaches developed below is that the initial structures that undergo filamentation have to produce during their evolution a set of well separated filaments. Breakup of the many-ring solutions results generally in strong interaction between filaments from different rings, and so is too complex to consider in the present approach.

Let us represent the fields in the form

$$E_m \simeq \sum_{n=1}^{N} B_{mn}(x,y) e^{i\vec{v}_n\vec{r}-(i/2)|\vec{v}_n|^2 z}, \quad m=1,2; \tag{34}$$

here $\vec{v}_n$ have a sense of the ''transverse velocities'' of the filaments. In other words $\vec{v}_n$ characterize the propagation directions of the solitary waves with respect to z axis. B_{mn} are assumed to be bell-shaped complex functions characterizing the filaments, localized near the points $\vec{r}_n=\vec{v}_n z$. N is the number of these filaments.

Substituting Eq. (34) into (31) gives for the angular momentum

$$\vec{L} \simeq \sum_{n=1}^{N} \int dxdy[\vec{r}\times\vec{v}_n](|B_{1n}|^2+2|B_{2n}|^2). \tag{35}$$

To get Eq. (35) we neglected the overlap of the tails of the filaments. We now assume that $\vec{r}$ can be replaced by $\vec{r}_n$ and taken outside the integral, which then reduces to q_n, the total energy of the filament, and so Eq. (35) becomes, for well-localized, well separated filaments

$$\vec{L} \simeq \sum_{n=1}^{N} \vec{r}_n \times q_n \vec{v}_n . \tag{36}$$

This is just the angular momentum of a set of spinless Newtonian particles with masses given by q_n. Under the same assumptions, $\vec{P} \simeq \Sigma_{n=1}^{N} q_n \vec{v}_n$, also the Newtonian form. If the initial linear and angular momenta are wholly transferred to the daughter filaments, these expressions for $\vec{L}$ and $\vec{P}$ must equate to those of the original ring soliton, i.e, $|\vec{L}|=|l|Q_0$ and $\vec{P}=0$.

We now make another simplifying assumption, restricting ourselves to cases where the breakup results in a set of the filaments with approximately equal energies. In this situation conservation of the two momenta obliges the filaments to move with nearly equal speeds ($|\vec{v}_n| \simeq v$) along paths tangent to the initial ring. Then in Eq. (36) we can estimate $|\vec{r}_n\times\vec{v}_n|=Rv$, where R characterizes the initial radius of the solitary solution. In practice we assigned R by an energy-weighted mean:

$$R=\frac{\int rdrr(A_1^2+2A_2^2)}{\int rdr(A_1^2+2A_2^2)}. \tag{37}$$

Finally, assuming that the entire energy and angular momentum are transferred to the filaments we get a very simple expression for the escape speed:

$$v \simeq \frac{|l|}{R}. \tag{38}$$

Plots of R versus κ for both our models are presented in Fig. 18. Equation (38) holds, under the stated assumptions, for both saturable and quadratic media. Before comparing it with numerical results, we consider an alternative Hamiltonian-based approach.

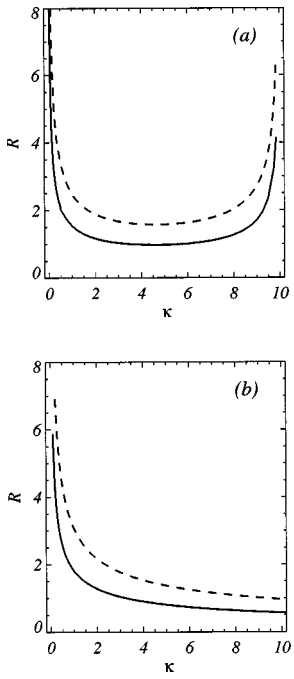

FIG. 18. Average radius of one-ring solutions vs κ. (a) Saturable medium, $\alpha=0.1$; (b) Quadratic media, $\beta=0$. Full and dashed lines correspond to $l=1$ and $l=2$, respectively.

Conservation of the Hamiltonian $H=\int dxdy\mathcal{H}$ suggests another way to estimate v. Substitution of Eq. (34) into H, under the same approximations as were used to get Eq. (36), gives

$$H_0\simeq\sum_{n=1}^{N} h_n+\frac{1}{2}\sum_{n=1}^{N} q_n v_n^2. \tag{39}$$

Equation (39) links the initial Hamiltonian H_0 with the sum of the ''intrinsic'' Hamiltonians h_n of the individual filaments calculated in their rest frames and of the ''kinetic energies'' arising from their transverse motion, the latter again conforming to the particle analog.

The Hamiltonians of the initial stationary solutions (7), (20) are respectively given by

$$H_0=-\kappa Q_0+2\pi\int rdr\left(f(A^2)A-\int_0^{A^2}duf(u)\right), \tag{40}$$

$$H_0=-\kappa Q_0+\pi\int rdrA_1^2A_2. \tag{41}$$

Considering the initial state as a composite of the final one, the last term in Eq. (39) can be interpreted as a ''negative binding energy,'' which induces breakup and transforms to kinetic energy of the fragments.

Supposing again that there are N identical filaments, i.e., $h_n\simeq h$, $q_n\simeq q$, we get the following formula for the speed:

$$v^2\simeq 2\left(\frac{H_0}{Q_0}-\frac{h}{q}\right). \tag{42}$$

For practical use of Eq. (42) we choose N that fixes $q\simeq Q_0/N$, and then we can find h for this q by using energy-Hamiltonian diagrams (see, e.g., [39]), assuming the filaments to be ground-state solitons. Note that in Eq. (42) the first term inside parentheses is fully defined by the initial conditions, but the second is an implicit function of N. Since Eq. (38) does not depend on N comparison between Eq. (38) and Eq. (42) leads to a direct estimate of the number N of daughter solitons without numerical simulation or stability analysis.

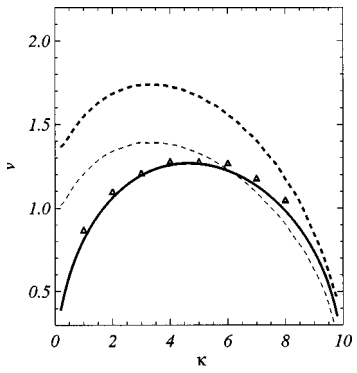

FIG. 19. ''Transverse velocities'' of filaments in saturable media vs κ for $l=2$, $\alpha=0.1$. Triangles mark results of the numerical simulation. Full line marks results gained through the angular momentum formula, Eq. (38). Dashed lines mark results gained through the Hamiltonian formula, Eq. (42). Thick and thin versions of the dashed lines correspond to the cases of 3 and 4 filaments respectively.

For our model systems we present in Figs. 19 and 20 examples of v versus κ obtained from the numerical simulation compared to the formulas given by Eqs. (38), (42). In both models there is near-perfect agreement of Eq. (38), based on angular momentum conservation, with numerical simulation. There is less good agreement with Eq. (42), based on the conservation of the Hamiltonian, though the qualitative behavior is correctly predicted. One reason for the discrepancy could be radiation, which we neglected in making these estimates. If so, it would seem that the radiation carries away energy and Hamiltonian more efficiently than linear or angular momentum. Alternatively, the daughter solitons may be in an excited state. Certainly, internal shape oscillations are apparent in the simulations and also in Fig. 17 (though exaggerated by the superposition of a finite num-

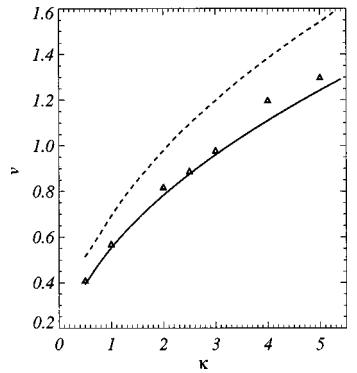

FIG. 20. ''Transverse velocities'' of filaments in quadratic media vs κ for $l=1$, $\beta=0$. Triangles mark results of the numerical simulation. Full line marks results gained through the angular momentum formula, Eq. (38). Dashed line marks results gained through the Hamiltonian formula, Eq. (42).

ber of images at discrete times). These questions demand more detailed investigation, which we postpone to future work.

The approaches presented above can be in fact applied to any initial field distribution that produces a set of well separated filaments with close intensities, e.g., they can be used to analyze breakup of Laguerre-Gaussian beams carrying orbital angular momentum.

In physical units Eq. (38) states that the angular divergence of the filaments is just the diffraction angle of a beam with radius $\rho = Rw$ multiplied by the order $|l|$ of the phase singularity,

$$v \simeq \frac{|l|\lambda}{2\pi\rho}, \tag{43}$$

where λ is the wavelength of the light (for the quadratic case, the SH field has half the wavelength but double the $|l|$ value, and so the divergence is the same for both fields). This link between a linear quantity, the diffraction angle, and the nonlinear phenomenon of azimuthal instability suggests an analogy with the linear approach to soliton theory developed in [40].

V. SUMMARY

Ringlike solutions with a phase dislocation nested at the center and exponentially decaying tails exist in self-focusing saturable and in quadratic media. They are quite different from the ''classical'' optical vortex soliton supported by a defocusing nonlinearity [5], which is a dark spot with a phase dislocation on a broad, stable, bright background. Dynamics of the solutions studied here is characterized by azimuthal modulational instability which leads to breakup of the rings into a set of the filaments. This sort of dynamics has already been experimentally observed, both in a saturable alkali vapor [30,31] and in photorefractive media [11]. This shows that these solitary solutions, some properties of which can be more or less rigorously studied theoretically, reflect the main features of the dynamics of input beams used in experiments.

Solitons have been observed to spiral around each other because of a balance between either in-phase [41] or incoherent [42] attraction and repulsion due to nonzero angular momentum. Here, in contrast, we have nearly free quasisolitons, with dynamics dominated by angular momentum conservation. Interaction forces may play a minor role in partitioning the energy among the filaments, but the daughter solitons rapidly cease to interact and fly off along straight-line trajectories tangentially to the initial ring without any spiraling. Note that a side view of the filaments in [30] shows rectilinear trajectories with no obvious evidence of any spiraling, so it seems possible to achieve such angular momentum dominated dynamics in practical experiments.

Initializing model equations (2),(19) with self-trapped beams with phase dislocation (plus noise) we demonstrated that their initial nonzero angular momentum transfers to the filaments and they fly out tangentially from the initial ring. We developed two semianalytic approaches to the filament dynamics, in analogy with classical mechanics, one of them based on Hamiltonian conservation and the other on conservation of angular momentum. Although both approaches give qualitatively valid estimates for the ''transverse velocity'' (angular divergence) of the filaments, the latter appears to be more general and gives also an excellent quantitative agreement with numerical results. The number N of daughter filaments is in most situations roughly twice the angular momentum index l, and thus depends relatively weakly on the other parameters. Taken together, the two approaches based on conservation laws yield an independent estimate for N in reasonable accord with estimates based on simulations and on stability analysis, both of which require considerable computational labor.

ACKNOWLEDGMENTS

We thank the authors of Refs. [5,23,29] for supplying copies of their manuscripts prior to publication. D.V.S. acknowledges financial support from the ORS. This work was partially supported by EPSRC under Grant No. GR/L 27916.

[1] R. Y. Chiao, E. Garmire, and C. H. Townes, Phys. Rev. Lett. **13**, 479 (1964).

[2] J. J. Rasmussen and K. Rypdal, Phys. Scr. **33**, 491 (1986).

[3] E. A. Kuznetsov, A. M. Rubenchik, and V. E. Zakharov, Phys. Rep. **142**, 103 (1986).

[4] E. A. Kuznetsov and S. K. Turytsin, Zh. Éksp. Teor. Fiz. **94**, 119 (1988) [Sov. Phys. JETP **38**, 1583 (1988)]; G. S. McDonald, K. S. Syed, and W. J. Firth, Opt. Commun. **96**, 281 (1993); C. T. Law and G. A. Swartzlander, Jr., Opt. Lett. **18**, 586 (1993); V. Tikhonenko, J. Christou, B. Luther-Davies, and Y. S. Kivshar, *ibid.* **21**, 1129 (1996); B. Luther-Davies, J. Christou, V. Tikhonenko, and Y. S. Kivshar, J. Opt. Soc. Am. B **14**, 3045 (1997).

[5] Y. S. Kivshar and B. Luther-Davies, Phys. Rep. **298**, 81 (1998).

[6] R. Schiek, J. Opt. Soc. Am. B **10**, 1848 (1993); M. J. Werner and P. D. Drummond, *ibid.* **10**, 2390 (1993); A. G. Kalocsai and J. W. Haus, Phys. Rev. A **49**, 574 (1994).

[7] C. R. Menyuk, R. Schiek, and L. Torner, J. Opt. Soc. Am. B **11**, 2434 (1994).

[8] D. E. Pelinovsky, A. V. Buryak, and Y. S. Kivshar, Phys. Rev. Lett. **75**, 591 (1995).

[9] W. E. Torruellas, Z. Wang, D. J. Hagan, E. W. VanStryland, G. I. Stegeman, L. Torner, and C. R. Menyuk, Phys. Rev. Lett. **74**, 5036 (1995); R. A. Fuerst, D. M. Baboiu, B. Lawrence, W. E. Torruellas, G. I. Stegeman, S. Trillo, and S. Wabnitz, *ibid.* **78**, 2756 (1997); A. DeRossi, S. Trillo, A. V. Buryak, and Y. S. Kivshar, Phys. Rev. E **56**, R4959 (1997); D. M. Baboiu and G. I. Stegeman, Opt. Lett. **23**, 31 (1998); D. V. Skryabin and W. J. Firth, Opt. Commun. **148**, 79 (1998).

[10] A. V. Mamaev, M. Saffman, D. Z. Anderson, and A. Zozulya, Phys. Rev. A **54**, 870 (1996); A. V. Mamaev, M. Saffman, and

A. Zozulya, Phys. Rev. Lett. **76**, 2262 (1996); M. F. Shih, Z. G. Chen, M. Mitchell, M. Segev, H. Lee, R. S. Feigelson, and J. P. Wilde, J. Opt. Soc. Am. B **14**, 3091 (1997).

[11] Z. Chen, M. Shih, M. Segev, D. W. Wilson, R. E. Muller, and P. D. Maker, Opt. Lett. **22**, 1751 (1997).

[12] L. Allen, M. W. Beijersbergen, R. J. C. Spreeuw, and J. P. Woerdman, Phys. Rev. A **45**, 8185 (1992); N. R. Heckenberg, R. McDuff, C. P. Smith, and A. G. White, Opt. Lett. **17**, 221 (1992); N. B. Simpson, K. Dholakia, L. Allen, and M. J. Padgett, *ibid.* **22**, 52 (1997); M. S. Soskin, V. N. Gorshkov, M. V. Vasnetsov, J. T. Mallos, and N. R. Heckenberg, Phys. Rev. A **56**, 4064 (1997) and references therein; D. Rozas, C. T. Law, and G. A. Swartzlander, J. Opt. Soc. Am. B **14**, 3054 (1997), and references therein.

[13] S. M. Barnett and L. Allen, Opt. Commun. **110**, 670 (1994).

[14] L. Gagnon and C. Paré, J. Opt. Soc. Am. B **8**, 601 (1991).

[15] A. E. Siegman, *Lasers* (University Science Book, Mill Valley, CA, 1986).

[16] H. A. Haus, Appl. Phys. Lett. **8**, 128 (1966); Z. K. Yankauskas, Izv. Vyssh. Uchebn. Zaved. Radiofiz. **96**, 412 (1966) [Sov. Radiophys. **9**, 261 (1966)].

[17] A. J. Glass, IEEE J. Quantum Electron. **10**, 705 (1974); V. I. Kruglov and R. A. Vlasov, Phys. Lett. **111A**, 401 (1985); V. I. Kruglov, V. M. Volkov, R. A. Vlasov, and V. V. Drits, J. Phys. A **21**, 4381 (1988); V. V. Afanasjev, Phys. Rev. E **52**, 3153 (1995).

[18] J. S. Hesthaven, J. P. Lynov, A. H. Nielsen, J. J. Rasmussen, M. R. Schmidt, E. G. Shapiro, and S. K. Turytsin, Phys. Fluids **7**, 2220 (1995).

[19] G. L. Alfimov, V. M. Eleonsky, N. E. Kulagin, L. M. Lehrmann, and V. P. Silin, Phys. Lett. A **138**, 443 (1989); Physica D **44**, 168 (1990).

[20] M. G. Vakhitov and A. A. Kolokolov, Izv. Vyssh. Uchebn. Zaved. Radiofiz. **16**, 1020 (1973) [Sov. Radiophys. **16**, 783 (1973)].

[21] J. M. Soto-Crespo, D. R. Heatley, E. M. Wright, and N. N. Akhmediev, Phys. Rev. A **44**, 636 (1991).

[22] H. He, M. J. Werner, and P. D. Drummond, Phys. Rev. E **54**, 896 (1996).

[23] J. P. Torres, J. M. Soto-Crespo, L. Torner, and D. V. Petrov, J. Opt. Soc. Am. B **15**, 625 (1998).

[24] D. V. Skryabin and W. J. Firth, Phys. Rev. E **58**, 1252 (1998).

[25] V. I. Kruglov, Y. A. Logvin, and V. M. Volkov, J. Mod. Opt. **39**, 2277 (1992).

[26] N. V. Vysotina, N. N. Rosanov, and V. A. Smirnov, Opt. Spectrosc. **76**, 774 (1994); N. N. Rosanov, Prog. Opt. **35**, 1 (1996).

[27] M. Quiroga-Teixeiro and H. Michinel, J. Opt. Soc. Am. B **14**, 2004 (1997).

[28] W. J. Firth and D. V. Skryabin, Phys. Rev. Lett. **79**, 2450 (1997).

[29] N. V. Vysotina, L. A. Nesterov, N. N. Rosanov, and V. A. Smirnov (unpublished).

[30] V. Tikhonenko, J. Christou, and B. Luther-Davies, J. Opt. Soc. Am. B **12**, 2046 (1995).

[31] V. Tikhonenko, J. Christou, and B. Luther-Davies, Phys. Rev. Lett. **76**, 2698 (1996).

[32] L. Torner and D. V. Petrov, J. Opt. Soc. Am. B **14**, 2017 (1997); D. V. Petrov and L. Torner, Opt. Quantum Electron. **29**, 1037 (1997).

[33] D. I. Abakarov, A. A. Akopyan, and S. I. Pekar, Zh. Éksp. Teor. Fiz. **52**, 463 (1967) [Sov. Phys. JETP **25**, 303 (1967)]; Y. Chen, IEEE J. Quantum Electron. **26**, 1236 (1991).

[34] J. Atai, Y. Chen, and J. M. Soto-Crespo, Phys. Rev. A **49**, R3170 (1994).

[35] The region of existence of these self-trapped solutions was incorrectly specified as $\kappa>0$ in Ref. [28].

[36] W. H. Press, S. A. Teukolsky, W. T. Vetterling, and B. P. Flannery, *Numerical Recipes in Fortran* (Cambridge University Press, Cambridge, 1992).

[37] N. N. Akhmediev, V. I. Korneev, and R. F. Nabiev, Opt. Lett. **17**, 393 (1992).

[38] K. Dholakia, N. B. Simpson, M. J. Padgett, and L. Allen, Phys. Rev. A **54**, R3742 (1996).

[39] N. N. Akhmediev and A. Ankievich, *Solitons: Nonlinear Pulses and Beams* (Chapman & Hall, London, 1997).

[40] A. W. Snyder, D. J. Mitchell, and Y. S. Kivshar, Mod. Phys. Lett. B **9**, 1479 (1995).

[41] L. Poladian, A. W. Snyder, and D. J. Mytchell, Opt. Commun. **85**, 59 (1991).

[42] M. Shih, M. Segev, and G. Salamo, Phys. Rev. Lett. **78**, 2551 (1997).